TU Delft

Delft University of Technology

Ground-based Wind Field Construction from Mode-S and ADS-B Data with a Novel Gas Particle Model

Sun, Junzi; Vû, Huy; Ellerbroek, Joost; Hoekstra, Jacco

Publication date
2017

Document Version
Final published version

Published in
Proceedings of the Seventh SESAR Innovation Days, 28th – 30th November 2017

Citation (APA)
Sun, J., Vû, H., Ellerbroek, J., & Hoekstra, J. (2017). Ground-based Wind Field Construction from Mode-S and ADS-B Data with a Novel Gas Particle Model. In *Proceedings of the Seventh SESAR Innovation Days, 28th – 30th November 2017: Belgrade, Serbia*

Important note
To cite this publication, please use the final published version (if applicable).
Please check the document version above.

Copyright
Other than for strictly personal use, it is not permitted to download, forward or distribute the text or part of it, without the consent of the author(s) and/or copyright holder(s), unless the work is under an open content license such as Creative Commons.

Takedown policy
Please contact us and provide details if you believe this document breaches copyrights.
We will remove access to the work immediately and investigate your claim.

This work is downloaded from Delft University of Technology.
For technical reasons the number of authors shown on this cover page is limited to a maximum of 10.

Ground-based Wind Field Construction from Mode-S and ADS-B Data with a Novel Gas Particle Model

Junzi Sun, Huy Vû, Joost Ellerbroek, Jacco Hoekstra
Control and Simulation, Faculty of Aerospace Engineering
Delft University of Technology, the Netherlands

***Abstract*—Wind is an important parameter in many air traffic management researches, as it often introduces significant uncertainties in aircraft performance studies and trajectory predictions. Obtaining accurate wind field information has always been a challenge due to the availability of weather sensors. Traditionally, there is no direct method to measure wind data at different altitudes with the exception of weather balloon systems that cannot be easily scaled. On the other hand, aircraft, which rely heavily on atmospheric data, can be part of atmospheric model itself. Aircraft can provide wind and temperature measurements to ground observers. In this paper, aircraft are considered as a moving sensor network established to re-construct the wind field on a larger scale. Based on the powerful open-source tool pyModeS, aircraft ground velocity and airspeed are decoded from ADS-B and Mode-S data respectively. Wind observations are then derived based on the difference of these two vectors. An innovative gas particle model is also developed so that the complete wind field can be constructed continuously based on these observations. The model can generate wind field in real-time and at all flight levels. Furthermore, the confidence of wind at any 4D position can be computed according to the proposed model method. Multiple self- and cross-validations are conducted to ensure the correctness and stability of the model, as well as the resulting wind field. This paper provides a series of novel methods, as well as open-source tools, that enable the research community using simple ADS-B/Mode-S receivers to construct accurate wind fields.**

Keywords - ADS-B, Mode-S, aviation weather, wind modeling, aircraft sensor network, gas particle model

I. Introduction

Using airplanes as weather sensors is a relatively new field in ATM and meteorological research. Traditionally, aircraft obtain weather updates from air traffic services to optimize their trajectory and speed, to best adapt to wind conditions, and to avoid areas of drastic weather conditions. These meteorological updates are mostly coming from ground-based operations, for example, radar surveillance, observation stations, or forecast systems [1], [2]. On the other hand, while an aircraft flies through an airspace, its local meteorological conditions can also be computed. Existing systems such as Aircraft Meteorological Data Relay (AMDAR) [3] and Meteorological Routine Air Report (MRAR) allow aircraft to down-link these meteorological data either through ACARS and Mode-S respectively. Air traffic controllers can combine these data with external sources to make better predictions of weather, which can then be updated and relayed to other aircraft.

Both AMDAR are MRAR are unencrypted broadcast data, which means that anyone can set up receivers to intercept these data. However, as part of ACARS, the legality of intercepting AMDAR is questionable in certain countries. As for MRAR, the amount of aircraft that broadcast this information is extremely limited. Most aircraft transponders choose not to enable this capacity and is also not interrogated by many ATC. Also, like other Mode-S data, the decoding for MRAR can be troublesome for the research community due to the closed design of downlink data structure.

Several previous studies have been proposed to use flight data from various sources to estimate wind conditions at the location of aircraft. They can be generally divided in three stages or categories:

1) *Estimation of wind from from ground based trajectory observation*: This concept assumes a quasi-constant wind velocity and aircraft airspeed during a turning maneuver. The wind velocity vector can then be estimated dynamically using multiple continuous observations of aircraft ground speed in combination with Bayesian filtering. Early in 1989, Hollister et al. [4] first proposed this method. Later on, Delahaye and Puechmorel, applied variations and extensions of such methodology [5], [6], [7]. Now that ADS-B transponders have been widely deployed, monitoring aircraft states through ADS-B has become a possiblity. De Leege et al. and De Jong et al. were the first to introduced the use of ADS-B data to solve this problem [8], [9].

2) *Estimation of aircraft local wind from Mode-S data*: Mode-S provides many additional aircraft states to ground control, complimenting radar or ADS-B data. A series of studies conducted by the Dutch Meteorological Institute presented by De Haan et al. constructed wind from Mode-S and MRAR data [10], [11]. Hrastovec and Solina also implemented a similar experimental method to achieve the same goal [12]. In addition to the previously mentioned direct wind information in MRAR, airspeed of aircraft are down-linked. The wind can be computed as the difference between aircraft airspeed and ground speed. De Haan also used such a method to calculate local wind data of aircraft [13].

3) *Wind field estimation based on multiple wind measurements*: While most of the above researches focused on deriving the local meteorological conditions of an aircraft, several of these studies also extended their methods to larger wind field or multiple aircraft scenario. For example, Hollister proposed the Hidden Markov model to update a wind grid based on measurement from multiple aircraft. Delahaye and De Leeg used non-linear Kalman filters on either radar or ADS-B data to obtain wind field. In additional to previously mention literatures, other methods also exist. For example, Hurter et al. used the least-squared method to construct wind field from multiple aircraft measurements [14], while Kapoor et al. implemented machine learning based on the Gaussian Process to predict and extrapolate wind field [15].

Based on the existing literature, researchers are also able to estimate wind vector using aircraft data. However, there are still areas missing in terms of constructing wind field based on measurements from aircraft. Unlike other types of direct sensor networks, using aircraft themselves as wind sensors has several disadvantages:

- Airplanes are moving objects. Therefore, the measurements derived from air traffic data have both temporal and spatial continuity and variance.
- As aircraft tend to fly along a predefined path, most measurements are concentrated along these flight paths. Except climbing or descending, aircraft also tend to fly at fixed cruise levels. This creates a high concentration of measurements along flight routes, alongside rare or no measurement in other spaces.
- The chaotic and temporal nature of wind makes the model highly non-persistent.
- Decoding airspeed from EHS entails a certain level of ambiguity and, thus, leads to errors in individual wind calculation.

The focus of this paper is to investigate a novel and relatively fast gas particle model that estimates real time wind field from observations of aircraft ground speed and airspeed gathered by a ADS-B/Mode-S receiver. The gas particle model can be used to estimate states of wind field and address the challenges caused by the dynamic and not evenly distributed observations. Tunable model-parameters can be used to produce confidence levels of wind field and to configure model persistence.

The crucial part of decoding ADS-B and Mode-S data are open-sourced by the authors of these paper. And the process of generating wind observations based on these data will be addressed. Within the framework of this paper, wind observations are first computed using the difference between ground speed (from ADS-B messages) and airspeed (derived from Mode-S messages) using open-source software pyModeS [16]. Then the observations are used by the particle model to construct the wind field and compute wind vector at any positions with confidence indicators. The results are first validated with external wind data source (i.e.: Global Forecast System datasets) for an extended period of time. Finally, the model is self-validated to examine variances and stabilities.

The remainder of the paper is structured as follows. Section two describes the process of obtaining wind observations. Section three presents the essentials of the gas particle model with simple examples. Section four details the large number of the experiments and validations conducted based the model. Finally, the discussion and conclusions are presented in sections five and six.

II. The wind observations

A simple ADS-B/Mode-S receiver is installed at the faculty of Aerospace Engineering at the Delft University of Technology. This device provides a constant stream of signals obtained from aircraft. Using open-source decoding library pyModeS, the ADS-B and Mode-S data that are collected can be used to derive wind observations for the particle model.

A. Processing of Mode-S data

Through Mode-S, different aircraft state information is downlinked to ground receivers. This information contains aircraft positions, velocities, operational parameters, and meteorological data, etc. The Mode-S transponder can maintain 256 different 56-bit wide Binary Data Store registers (BDS) that can be interrogated by ATC. These registers are indicated by two-digit hexadecimal numbers that can be requested via 25 different downlink formats (DF). Information in these registers are updated with a minimum interval specified by ICAO.

Among all these downlink formats, ADS-B is transmitted via DF17 (or DF18), while Mode-S EHS/MRAR is transmitted via DF20 and DF21. Decoding of ADS-B messages is well documented. However, the decoding of Mode-S data is much more challenging. The challenges include determining the source of aircraft (ICAO address), the content of message (from BDS code), and the quality of the content (certainty of the values).

Aircraft ICAO addresses can be determined by the reverse parity check of the Mode-S message (DF04, DF05, DF20, and DF21). Correct ICAO addresses can only be obtained when a signal is not corrupt. If a message is corrupt (e.g. one or more bits are flipped), it will result in an incorrect ICAO address. However, by cross-referencing resulting ICAO addresses with ADS-B streaming, error messages can be discovered.

The second challenge is that, unlike ADS-B, Mode-S messages do not contain any information on their message types (i.e. BDS codes). This is because only the interrogating ATC knows the target aircraft and what to expected in the downlink message. Such a lack of transparency in Mode-S design poses the biggest challenge in making use of these open data. With the latest version of pyModeS, much of this data is finally unveiled.

Briefly, in pyModeS, the BDS code is determined by checking several signification status bits and evaluating possible values contained in the messages. A status bit indicates whether its related register field (aircraft parameter) is available in the message. This is implemented as follows: When a status bit is set to zero, all related content bits should be zero as well. Messages with different BDS codes usually have different signification status bits. Thus, multiple checks assuming different message types need to be performed to evaluate all possible types or a combination of types. It may occur that a message matches multiple BDS codes. In this paper, only uniquely identified messages are kept and used for the propose particle model.

The last challenge is the quality of the content. Values decoded from corrected messages may be incorrect due to aircraft measurements or transmission errors. For now, no additional filtering is applied in order to provide the direct computation of wind observations. A good design of wind field model needs to cope with this uncertainty, in addition to the errors from incorrect BDS identifications.

B. Compute wind vectors

Figure 1 shows the relationship between true airspeed, ground speed, and wind. The ground speed vector $\boldsymbol{V}_g$ given by Equation 1 is the sum of the true airspeed vector $\boldsymbol{V}_a$ and wind vector $\boldsymbol{W}$. χ_g, χ_a, and χ_w are the ground speed vector angle (track angle), airspeed vector angle (heading) and wind vector angle with respect to the true north respectively.

$$\boldsymbol{V}_g = V_a + W \tag{1}$$

To simplify calculations in equation 1, the vectors $\boldsymbol{V}_g$, $\boldsymbol{V}_a$, and $\boldsymbol{W}$ are decomposed into a west-east component V_x and a south-north component V_y. The decompositions are calculated using Equation 2.

$$\begin{aligned} V_x &= \boldsymbol{V} sin(\chi) \\ V_y &= \boldsymbol{V} cos(\chi) \end{aligned} \tag{2}$$

Wind components can then be calculated with Equation 3.

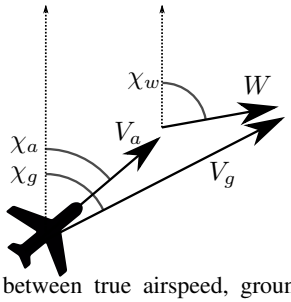

Figure 1: Relation between true airspeed, ground speed, and wind vector

$$\begin{aligned} W_x &= V_{g_x} - V_{a_x} \\ W_y &= V_{g_y} - V_{a_y} \end{aligned} \tag{3}$$

To calculate the wind, the airspeed and ground speed should first be determined. This can be done using ADS-B and Mode-S data. In Table I, the relevant variables from ADS-B and Mode-S are given.

TABLE I: Usable information from ADS-B and Mode-S

ADS-B	BDS 5,0	BDS 6,0	MRAR
Track angle	Track angle	Magnetic heading	Wind speed
Ground speed	Ground speed	Indicated airspeed	Wind direction
Position	True airspeed	Mach number	Air temperature
Pressure alt.			Static pressure
Geometric alt.			

The wind vector can then be determined as follows:

- Other than the ground speed vectors from ADS-B directly, the ground speed, true airspeed, and track angle are also available in BDS 5,0 messages.
- In BDS 6,0, the indicated airspeed is available. This can, in turn, be converted into true airspeed, assuming that indicated airspeed is equal to the calibrated airspeed. Under the ISA condition, the true airspeed can be calculated using Equation 4.

$$V_{TAS} = \left\{ \frac{2\kappa}{\kappa-1} \frac{p}{\rho} \left[\left\{ 1 + \frac{p_0}{p} \left[\left(1 + \frac{\kappa-1}{2\kappa} \frac{\rho_0}{p_0} V_{CAS}^2 \right)^{\frac{\kappa}{\kappa-1}} - 1 \right] \right\}^{\frac{\kappa-1}{\kappa}} - 1 \right] \right\}^{\frac{1}{2}} \tag{4}$$

where p and ρ are pressure and air density respectively. κ is the specific heat ratio of 1.4. Parameters with subscript 0 represent their values at sea level. Furthermore, since BDS 6,0 also contains the Mach number, the true airspeed can also be derived more accurately with Equation 5.

$$\begin{aligned} V_{TAS} &= \frac{V_{CAS}}{f(p,M)} \sqrt{\frac{\rho_0}{\rho}} \\ f(p,M) &= 1 + \frac{1}{8}\left(1 - \frac{p}{p_0}\right) M^2 \\ &\quad + \frac{3}{640}\left(1 - 10\frac{p}{p_0} + 9\frac{p^2}{p_0^2}\right) M^4 \end{aligned} \tag{5}$$

- In order to determine the airspeed vector, heading is required. Aircraft magnetic heading can be obtained via BDS 6,0. However, the heading information refers to the magnetic heading of aircraft, which should be converted into true north depending on the location of the aircraft. [1]
- When BDS 4,4 (MRAR) messages are detected, direct meteorological information on wind can be decoded.

III. The Particle Model

The idea behind the proposed particle model is to mimic gas particles in nature. The particles are modeled to carry the states of a wind measurement. Particles are first generated when a new measurement of wind is obtained and decay over time according to a certain parameterized kernel function. Using a stochastic process model, these particle propagates within the airspace. Wind fields are constructed by combining the weighted states of all neighboring particles. The propagation of particles allows for wind at areas of low measurement density to be computed. The following section will be dedicated to a more detailed explanation of the model, methods, and kernel functions used to compute wind field and confidences.

A. Measurement array

A single wind measurement is a 2D vector represented by a west-east w_x and a south-north w_y component, in 3D space (x, y, z). The measurement array consists of all wind measurements from different aircraft at a given time, defined as $[X, Y, Z, W_x, W_y]$.

B. Particles

A particle is defined as a point object that carries the states of wind. Particle states consist of position (p_x, p_y, p_z), origin (p_{x0}, p_{y0}, p_{z0}), carried wind states (s_{wx}, s_{wy}), and age (τ).

Particles are generated when new wind measurements are observed (computed). For any new measurement vector $[X, Y, Z, W_x, W_y]$ with M measurements, N number of particles are created for each measurement. The total number of $M \times N$ particles is generated from a multivariate normal distribution, using the aircraft position as the mean value.

$$\begin{pmatrix} p_{x,mn} \\ p_{y,mn} \\ p_{z,mn} \end{pmatrix} \sim \mathcal{N}\left(\begin{bmatrix} x_m \\ y_m \\ z_m \end{bmatrix}, \begin{bmatrix} \sigma_x^2, & 0, & 0 \\ 0, & \sigma_y^2, & 0 \\ 0, & 0, & \sigma_z^2 \end{bmatrix} \right) \tag{6}$$

The carried states of particles are also assigned a small variance that represents the uncertainty of the wind measurement:

$$\begin{pmatrix} s_{wx,mn} \\ s_{wy,mn} \end{pmatrix} \sim \mathcal{N}\left(\begin{bmatrix} w_{x,m} \\ w_{y,m} \end{bmatrix}, \begin{bmatrix} \sigma_{wx}^2, & 0 \\ 0, & \sigma_{wy}^2 \end{bmatrix} \right) \tag{7}$$

As an example, Figure 2 displays the measurement vectors in solid arrows and generated particles in tiny vectors. (Note that only 10% of the particle samples are shown for a more clear illustration.) The plot shows the 2D projection of the X-Y plane. The dashed circles indicate the variance of particle positions in relation to the measurement location.

[1] The magnetic declination in the Netherlands is only around 1 degree. Thus, for simplification purpose, in later datasets, the heading is assumed to be equal to the magnetic heading.

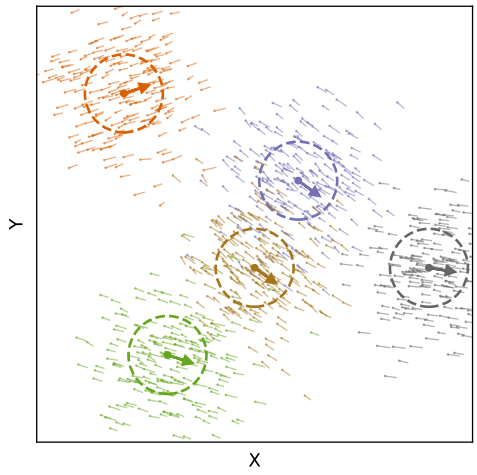

Figure 2: Wind measurements and corresponding particles

C. Particle motion model

Particle motion follows a Gaussian random walk model that takes into consideration of the actual wind vector (s_{wx}, s_{wy}). At each step update, the particle age (τ) increases. The following equation describes the motion model of a particle.

$$\begin{aligned} p_{(x,y,z),t+1} &= p_{(x,y,z),t} + \epsilon_{(x,y,z)} \\ \epsilon_{(x,y)} &\sim \mathcal{N}\left(\begin{bmatrix} k \cdot s_{wx} \\ k \cdot s_{wy} \end{bmatrix}, \begin{bmatrix} \sigma_{px}^2, & 0 \\ 0, & \sigma_{py}^2 \end{bmatrix}, \right) \\ \epsilon_z &\sim \mathcal{N}(0, \sigma_z^2) \end{aligned} \tag{8}$$

The step factor ϵ is different in the horizontal and vertical direction. Horizontally, the term $k \cdot s_{(wx,wy)}$ allows the random walk executed with a small biased along the direction of wind, with a scaling factor k. Choosing a larger k allows the propagation becomes more biased toward the wind direction. Vertically, the propagation follows a zero mean Gaussian walk. The particle motion model is illustrated in Figure 3, where two projections (X-Y and X-Z) of a possible particle update are shown. The red dot represents the position $p_{(x,y,z),t}$, while the probability of the next position $p_{(x,y,z),t+1}$ is shown by the contour plot. The vector equals to $\mathbb{E}\left[\epsilon_{(x,y,z)}\right]$. Also note that the length of vectors and variances are not to their real scale. In reality, $k \cdot s_w$ is much smaller than variances.

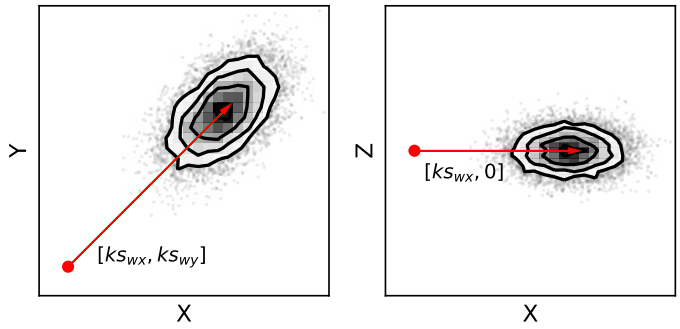

Figure 3: Possible random update of a particle position

The updates of particles follow the Gaussian random walk as shown in Figure 4, where several possible 100-step random walks of a particle (with origin $[0, 0, 0]$) are illustrated. Different trajectories are distinguished by different colors.

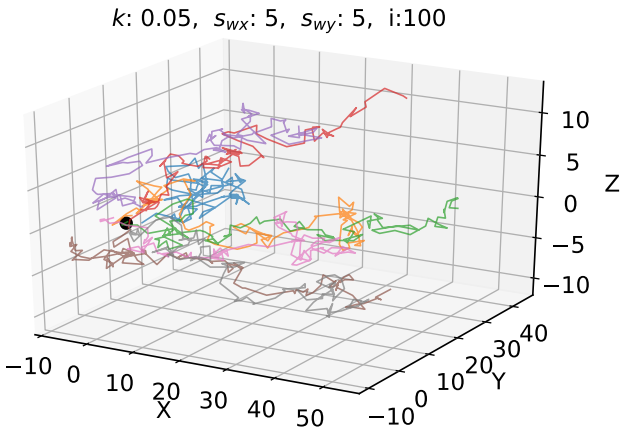

Figure 4: Examples of particle random walks in 3D

D. Wind field construction

The wind field is represented by a grid of equally spaced coordinates, which has the size of $I \times J \times K$. Numbers I, J, and K represent the number of grid points at each axis. From each grid point (x_i, y_j, z_k), the wind is constructed using the weighted wind state values from its neighboring P number of particles:

$$\begin{bmatrix} W_{x,(i,j,k)} \\ W_{y,(i,j,k)} \end{bmatrix} = \frac{1}{\sum_{p=1}^{P} \omega_p} \times \sum_{p=1}^{P} \left(\omega_p * \begin{bmatrix} s_{wx,p} \\ s_{wy,p} \end{bmatrix} \right) \tag{9}$$

The ω_p is the weight of each particle that is computed based on the product of two kernel functions. Function $f_d(\cdot)$ draws an exponential relationship between weight and distance between the particle and the coordinate. Function $f_o(\cdot)$ defines the weight of the particles and depends on distance to their origins. Function $f_a(\cdot)$ expresses the similar relationship between weight and particle age.

$$\omega_p = f_d(d) \times f_o(d_0) \times f_a(\tau) \tag{10}$$

$$f_d(d) = \exp\left(-\frac{d^2}{2C_d^2}\right) \tag{11}$$

$$f_o(d0) = \exp\left(-\frac{d_0^2}{2C_o^2}\right) \tag{12}$$

$$f_a(\tau) = \exp\left(-\frac{\tau^2}{2C_a^2}\right) \tag{13}$$

Here, d represents the spatial distance between particle and grid point. C_d C_o, and C_a are control parameters for the kernel functions $f_d(\cdot)$, $f_o(\cdot)$, and $f_a(\cdot)$.

Figure 5 displays the constructed wind field from previously generated particles, at time-step zero. At each grid point, the wind vector is shown in solid arrows. Grid points with no information yet are presented in scattered circles.

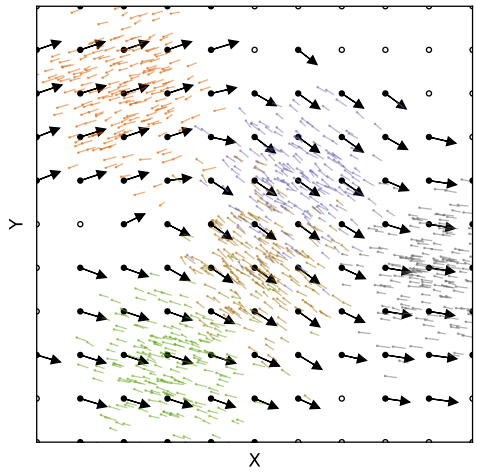

Figure 5: Wind field constructed from particles (10% particle samples illustrated)

E. Wind field confidence model

The confidence level of each grid point in the wind field is computed as the combination of confidence functions that are based on several independent factors. These factors are:
1) the number of particles in the vicinity of the grid point (N)
2) the mean distances between particles and the grid point (D)
3) the homogeneity of wind states carried by particles (H)
4) the strength of particles due to decaying function (S)

1) Particle numbers and distances: The idea behind these two confidence parameters is to give the wind field a higher confidence value where more and closer measurements are observed. On the contrary, areas that are far from flight trajectories tend to have less reachable particles and should yield a lower confidence value.

2) Homogeneity of carried states: The level of homogeneity refers to the similarity of particle states. It essentially indicates whether different measurements propagated from a nearby area indicate similar evidence of wind vectors. It is computed as the norm (spectral norm) of the covariance matrix of two wind states of all particles:

$$\begin{aligned} \Sigma &= Cov(S_{wx}, S_{wy}) \\ H &= \|\Sigma\|_2 = \sqrt{\lambda_{max}(\Sigma^T \Sigma)} \end{aligned} \tag{14}$$

where the λ_{max} represents the largest eigenvalue of a matrix.

3) Particle strength: Since a particle's creation, its age parameter (τ) increases at each step of propagation. The decaying strength obtained by Equation 13 regularizes not only the weights of particles in wind calculation, but also the confidence. Mean strength of all neighborhood particles are calculated as follows:

$$S = \frac{1}{N} \sum_{p=1}^{P} f_a(\tau_p) \tag{15}$$

4) Normalized and combined confidence: Values from all four confidence factors all have a distinct range. It is important to normalize these factors into the same range. A linear scaler is used to covert all values of each factor into $(0, 1)$ range.

$$s(x) = \frac{x - \min(X)}{\max(X) - \min(X)} \tag{16}$$

At any given time, the confidence vectors that represent all wind grid points are: N, D, H, and S. Then, the combined confidence is expressed as:

$$C = mean\big\{s(N), s(D), s(H), s(S)\big\} \tag{17}$$

Figure 6 illustrates the confidence contour plot based on previously defined calculations. Areas in the plot in darker colors represent higher levels of confidence.

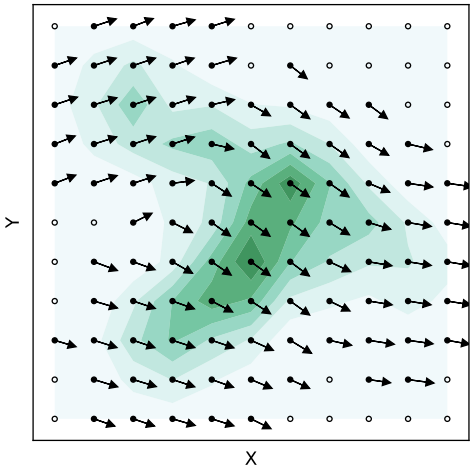

Figure 6: Wind field construction with confidence plot

F. Compute wind at any points

It is worth pointing out that the particle model runs independently of a pre-defined grid. When looking at the model as a dynamic object, particles are generated as measurements are observed. They are propagated independently from then on. This property allows us not to store the measurement and still be able to compute wind at any given time and space.

Hence, wind states from this particle model are not limited to any symmetric grid points. Values can be computed at any point or any set of points. Equation 9 can be used at all locations to produce accurate wind state information, as long as a sufficient number of particles exist in the neighborhood of these locations. The confidence levles can also be calculated in the same fashion.

IV. Experiments and Results

Firstly, a small data set from ADS-B and Mode-S are combined and used as wind observations as a means to generate the test wind field. Results are illustrated as a sampled wind grid. Later on, different validation criteria are proposed, and comparison experiments are conducted to examine the model and related results.

From ADS-B and Mode-S data, wind observations are calculated for the area that is covered by our ADS-B/Mode-S antenna. The area is about 600 kilometers in diameter and located around Delft, the Netherlands, as shown in Figure 7. Based on a one-hour continuous streaming of measurement data, wind vectors are computed on a 3D grid consisting of both horizontal and vertical points.

A. Constructing the wind field

The dataset consists of one hour of wind data obtained, from 11:30 to 12:30 hours on July 27, 2017. In total, around 87,600 wind measurements were generated during this one-hour period. In Figure 7, the distributions of wind observations are displayed both horizontally and vertically.

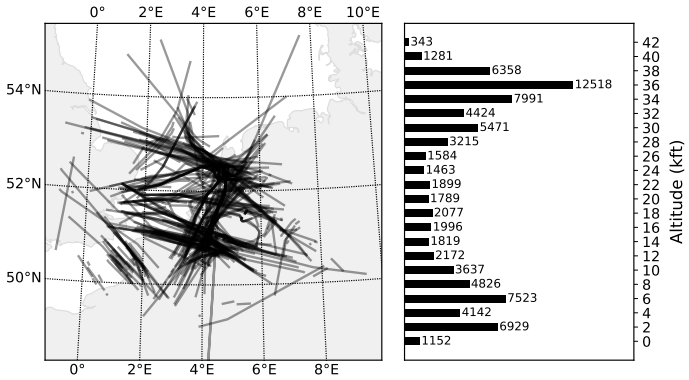

Figure 7: Wind data ground projections and vertical distributions

In this figure, the plot on the left hand side illustrates the ground projection of all observations. On the right hand side, the plot shows a histogram with the number of observations per 2,000 feet altitude. It is apparent that horizontally, the measurements are highly concentrated along flight routes. Vertically, the majority of the observations are at cruise altitudes and lower approaching altitudes.

Despite the horizontal location of the observations, the statistic of wind at different altitudes can be computed, as shown in Figure 8.

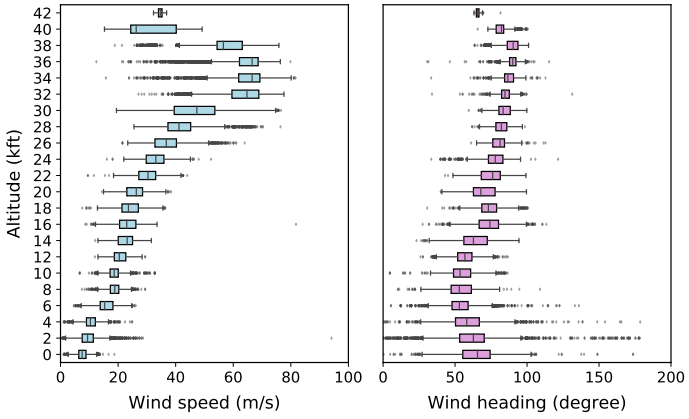

Figure 8: Wind speed and direction distributed at all flight levels

During this hour, it can furthermore be observed that wind generally comes from a west or south-west direction, but with different levels of velocities at different altitude levels. The time-spatial variate wind state also leads to variability in both wind velocity and direction at each altitude. Both Figure 7 and 8 illustrate the challenges of using aircraft as sensors to model atmospheric conditions, there being: 1) high non-uniform distribution, and 2) large variation in the time-spatial domain.

To simulate a real-time run of the model, these recorded wind data are streamed to the particle model using the original sequence based on the data time-stamp. Each second, there are around 11 wind observations on average computed by the receiver.

The entire area is converted with Cartesian coordinates centered at the location of receiver (latitude: 51.99°N, longitude: 4.37°E). For illustrative purposes, the horizontal visualization of wind grid size is set to 10 x 10, where each set of adjacent points are 60 km apart. Vertically, 12 equally separated flight levels are chosen for visualization. A snapshot of the wind grid at 12:00 hours is shown in Figure 9.

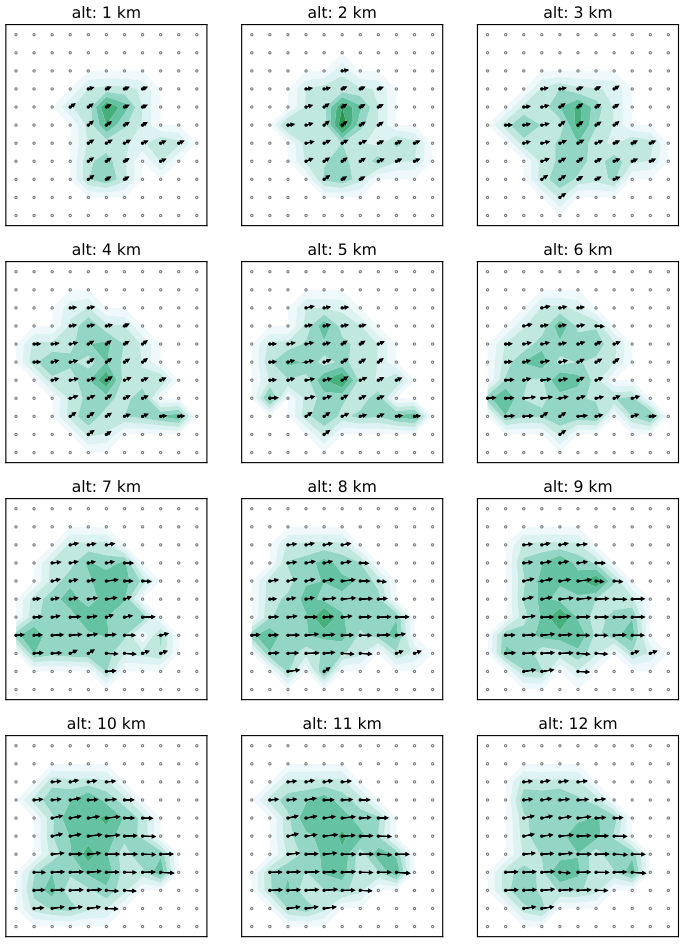

Figure 9: Wind grid at 12 different altitude levels

Visually, it can be ascertained that wind speed increases with increasing altitude. At lower altitudes, the wind generally comes from a south-west direction, while, at higher altitudes, wind generally comes from a westerly direction. Both speed and direction trends correspond with the observations from Figure 8. To further validate the accuracy of the results, several additional methods are addressed below.

B. Validation of particle model

The validation of the particle model is focused on two indicators: correctness and variability. The level of correctness can be examined against data from existing meteorological models. Global Forecast System (GFS) Analysis data are used for this purpose [2]. Variability can be caused by both the uncertainty in the model itself and the quality of data. Firstly, all particle generations and propagations follow a stochastic process. At each run and each step, the states of each individual

particle cannot be predicted. Secondly, wind measurements from aircraft also carry their own uncertainties.

To validate the model variation, multiple runs are performed for the same data. Differences in the resulting wind grid are compared. To validate the data variation, a complete dataset is sampled into different sizes of test datasets. Then, the results are compared with those from the complete dataset.

1) Correctness: To improve the quality in correctness validation, a much larger number of wind data samples across an entire week are used. GFS Analysis data provide global atmospheric re-analysis of all vertical levels at the highest resolution of 0.25 degrees latitudinal and longitudinal, at 00:00, 06:00, 12:00, and 18:00 hour each day. A wind observation dataset is aggregated that contains seven days of one-hour data computed around these hours from GFS, lasting from the 24th to 30th of July, 2017.

At a GFS hour (00:00, 06:00, 12:00, or 18:00), spot values and average values are computed. The spot value is the wind grid computed from the particle model at the exact GFS hour. The average values are computed as the mean of the hour around GFS hour (per minute, +/- 30 minute of wind grids).

To compare the difference in wind vectors from GFS and the particle model at the same position and time, two distance matrices - *angular difference* and *magnitude difference* - are calculated at each GFS hour.

The angular difference is computed as

$$\Delta\theta = \arccos\left(\frac{\boldsymbol{V}_{pm}\cdot\boldsymbol{V}_{gfs}}{\|\boldsymbol{V}_{pm}\|\cdot\|\boldsymbol{V}_{gfs}\|}\right) \tag{18}$$

where V_{pm} and V_{gfs} are the two wind vectors computed by the particle model and extracted from GFS respectively. $\Delta\theta$ is is the angle in degrees between two wind vectors with a range of $[0, 180]$. The smaller the $\Delta\theta$, the smaller the angular difference between the two wind vectors.

The magnitude difference is computed as the absolute difference of wind vectors:

$$\Delta V = \text{abs}(\|\boldsymbol{V}_{pm}\| - \|\boldsymbol{V}_{gfs}\|) \tag{19}$$

where the smaller the value, the smaller the difference between the two results.

Table II summarizes the results of the 7-day mean angular and magnitude differences between the wind field generated from the particle model and GFS data. The analysis is divided in two parts - part one, with up to gentle breeze wind (less than 10 m/s) and, part two, with higher speed wind (greater than 10 m/s). This distinction is needed because that small variability can cause large relative differences in low wind conditions. If analyze without such consideration, the low wind difference could be simply considered as outliers.

Both the spot value and average value are generated from the particle mode to compare with the GFS. They are also illustrated in box-plots in Figure 10. Within this 7-day data sample, the mean angular difference of the two wind fields is around 20 degrees for low speed wind and around 10 degrees for higher wind speeds. The magnitude difference is around 4-5 m/s as compared to around 20 m/s average wind speed.

When using a one hour (60 sample) average, the differences become small, but not significantly different. This is due to the fact that the particle model is already considering historical wind measurement as a result of the decaying factor. For example, in this experimental setting, historical observations of up to one minute still persist in the particle model.

It is apparent that for low wind speeds, the results are less aligned with the GFS data. However, this does not mean that the results are less accurate. Rather, the the wind information generated by the GFS model is smoothed and interpolated over much larger periods of time and areas.

TABLE II: Mean grid angular and magnitude distance

	$v_w \leq 10m/s$				$v_w > 10m/s$			
	spot		average		spot		average	
Date time	$\Delta\theta$	ΔV	$\Delta\theta$	ΔV	$\Delta\theta$	ΔV	$\Delta\theta$	ΔV
2017-07-24 00H	23.22	4.09	26.42	3.18	18.96	7.64	10.75	5.26
2017-07-24 06H	56.31	2.97	43.79	2.03	21.03	6.38	14.45	6.11
2017-07-24 12H	36.46	2.66	30.14	2.06	13.80	5.80	8.30	4.97
2017-07-24 18H	22.02	2.52	20.13	1.92	9.71	5.02	8.28	3.49
2017-07-25 00H	27.85	7.04	19.54	2.20	14.81	4.57	9.50	3.71
2017-07-25 06H	14.84	2.11	13.50	2.60	12.03	3.56	9.03	2.47
2017-07-25 12H	19.52	1.97	14.29	2.43	12.69	2.12	9.30	2.06
2017-07-25 18H	29.71	2.82	20.70	2.24	17.02	2.71	11.46	2.27
2017-07-26 00H	18.39	3.53	27.14	3.74	11.82	7.89	8.87	5.76
2017-07-26 06H	26.14	4.11	28.77	3.11	9.12	5.48	7.96	3.88
2017-07-26 12H	23.71	1.98	18.50	1.88	16.56	3.57	14.53	2.51
2017-07-26 18H	22.22	4.12	20.21	3.31	13.25	3.92	9.48	2.35
2017-07-27 00H	16.87	3.79	15.71	6.98	10.95	4.84	8.05	3.77
2017-07-27 06H	20.73	5.43	14.84	6.06	10.75	5.58	7.70	4.12
2017-07-27 12H	9.42	8.13	9.91	5.70	8.55	6.43	5.92	5.13
2017-07-27 18H	11.19	3.28	12.97	4.23	7.40	6.68	8.15	4.46
2017-07-28 00H	17.11	3.21	17.05	6.76	8.29	8.85	8.21	6.11
2017-07-28 06H	13.70	5.15	30.79	6.15	6.00	6.11	5.62	5.19
2017-07-28 12H	13.58	5.38	30.10	8.48	6.04	5.78	7.82	4.86
2017-07-28 18H	12.04	7.08	11.46	6.55	9.50	3.43	7.85	3.13
2017-07-29 00H	45.10	13.04	48.62	10.00	10.58	5.10	8.35	3.81
2017-07-29 06H	25.36	9.34	28.88	11.60	5.35	4.57	4.91	4.25
2017-07-29 12H	12.45	6.00	14.61	9.55	5.30	3.83	3.16	3.26
2017-07-29 18H	19.82	9.84	15.93	10.84	8.50	3.75	5.05	3.27
2017-07-30 00H	37.08	9.44	45.83	10.13	6.66	5.11	5.34	3.69
2017-07-30 06H	18.68	11.31	24.54	10.66	6.21	5.34	4.67	4.26
2017-07-30 12H	17.89	5.44	11.02	6.96	8.01	4.59	3.75	3.54
2017-07-30 18H	33.50	5.15	25.26	7.91	5.74	4.63	3.73	3.96

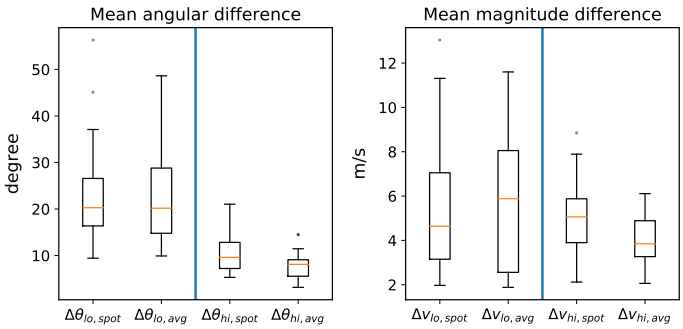

Figure 10: Mean wind gird angular and magnitude difference

2) Model variation: As previously stated, there is a certain level of the randomness in the particle model. The advantage of such randomness is that the model mimics and copes with the uncertainty of wind. With a large amount of particles, the general trend of wind is (hopefully) stable. To study whether the randomness of particles effects the wind field, as well as the level of the influence, the same example in Section IV-A is used with multiple runs of the particle model. The wind field at 12:00 hour (as shown in Figure 9) is computed at the end of each run.

In Figure 11, the distribution of standard deviations of wind grid speed and heading among 100 runs is displayed. Among these runs, the difference is almost negligible, namely less than

one degree for heading and 1 m/s for magnitude. [2] Using box-plots, the baseline variance is also illustrated for later comparisons.

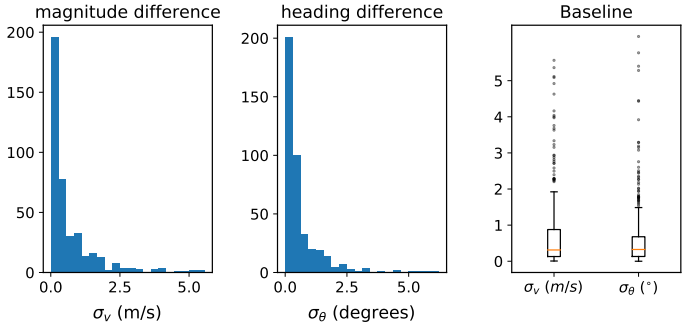

Figure 11: Standard deviation of wind speeds and headings of 100 runs

3) Data variation: Another important validation is to determine how the quality of observation data effects the wind field estimation. More precisely, it is necessary to ascertain whether the wind grid would be different if some percentage of the observed data are not available. To study this effect, the previous dataset is randomly sampled into several new datasets that contain 90%, 70%, 50%, 30%, and 10% of the total wind observations. Then, the same processes are run to create five different wind fields at 12:00 hour.

Figure 12 illustrates the wind grid estimated at the altitude level of 12km when different percentages of sampled data are used. From the first plot to the last, it is obvious that with increasing observation data samples, the size of estimated wind field is increased, together with an increased level of confidence. Visually, it is already possible to observe that the magnitude and headings of wind field are quite similar.

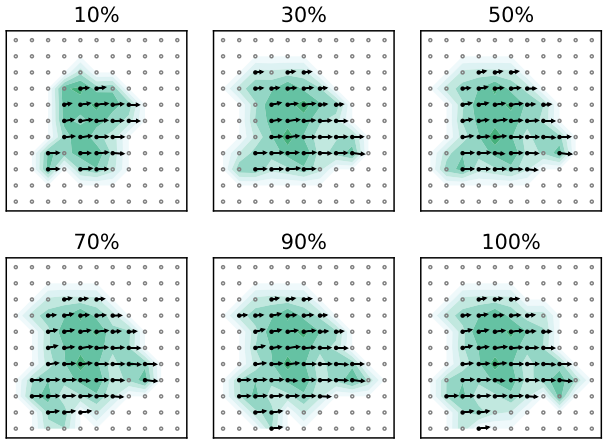

Figure 12: Wind field at a 12km altitude from different samples

In order to quantify the differences, mean heading and magnitude differences from the entire grid (including all altitude levels) of all wind vectors are compared with the results from the complete data, being shown in Figure 13.

It is apparent that the comparison with box-plots confirms the previous observation. Compared to the baseline variance of

[2]Grid points with higher variances are usually along the boundary regions with fewer particles.

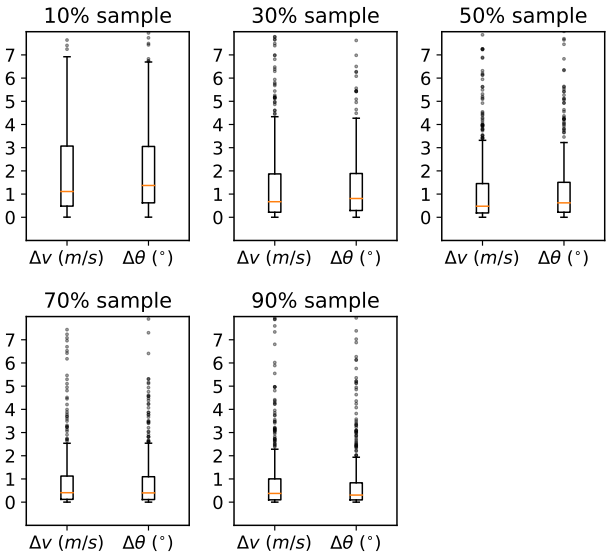

Figure 13: Grid magnitude and heading difference due to sampling

the model as shown in Figure 11, we can infer that with a loss of up to 50% of the total data, the differences are still within the acceptable range. This test indicates that, within a reasonable percentage of data uncertainty, the particle model can always obtain relatively stable wind field results.

4) Error resistance: The factor that effects the stability and correctness most is the fundamental measurement error in raw data. It is apparent that with a better accuracy in wind observations, the wind field can be better re-constructed. In Section II, from Mode-S and ADS-B data, different inference methods were implemented that trying to produce a higher level of wind accuracy. However, there is no reference data to check the correctness of the computed wind vectors themselves at this stage.

To study how errors in data would affect the wind field, a percentage of the dataset is replaced with random wind vectors that are uniformly distributed between the minimum and maximum wind speeds with headings between 0 and 360 degrees. In Figure 14, wind grid differences between no assumed error and data error rates of 2%, 4%, 6%, 8%, 10%, and 15% are shown.

With such a aggressive error model, the particle model can maintain a reasonably correct wind field with up to an error rate of approximately 5%. One can further infer that if the magnitude and heading errors are small (in another words, wind observations distributed close to their true values), the particle model would be able to handle an even larger percentage of data error.

V. Discussion

The introduction to this paper indicates four challenges posed by using aircraft as a sensor network to construct wind fields. Throughout the paper, methods and models are proposed to address those challenges.

The source - wind observations - remains the most important factor that influences the results. Without going into much detail, the computation of aircraft true airspeed in pyModeS is a complicated task. The challenge is not only the decoding of BDS 5,0 and 6,0 messages, but rather a complete identification

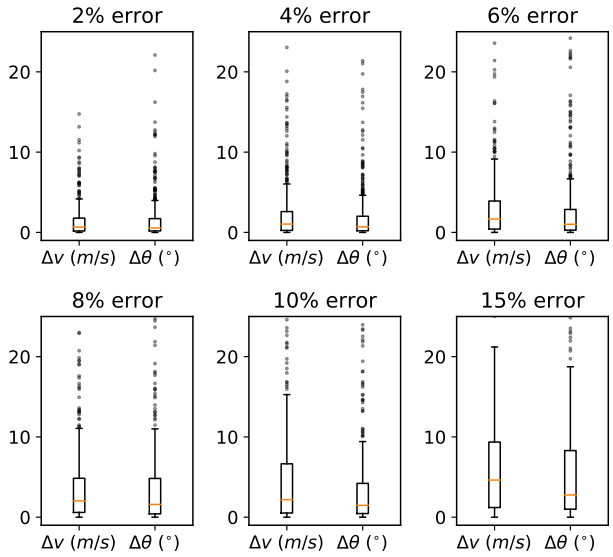

Figure 14: Grid magnitude and heading difference due to error

process of the entire Mode-S family of messages. As a third-party observer without the knowledge of Mode-S interrogations, the decoding is extremely complex. Developed by the the authors of this paper and supported by open-source community, pyModeS is an effective tool to solve this problem. Sophisticated identification processes can be found in the source code of the software as referenced.

Remaining challenges includes constructing a model that is able to cope with the chaotic nature of wind, moving sensors (aircraft), and extreme non-uniformly distributed observations. The particle model proposed in this paper addresses the stochastic characteristic of wind through particles, while maintaining the stability through the use of relatively large particle numbers. One must not confuse the model with Particle Filtering. The particle model mimics the gas particles' stochastic motions to propagate wind information (not actual wind) to their surrounding areas. Using the propagated information, wind filed in areas with less (or no) measurements can be estimated. Parameters on particle propagation and decaying can be tunned in order to control performance. These parameters are set empirically in this paper. However, for future work, an automatic parameter tunning method shall also be constructed.

As a novel approach, there are still a few remaining future developments. For example, together with wind, air temperature field can also be computed using Mode-S data. Since this paper is focused on the concept of the particle model, temperature has not been included in the scope of this paper. Air temperatures are generally more stable and evenly distributed spatially. Hence, using the same particle model with addition temperature state, a similar field can be generated in parallel.

VI. Conclusions

With the increasing accessibility of open ATM data from ADS-B and Mode-S, as well as related open-source decoding library development, exciting new possibilities for research are made available to the open research community. This paper proposes an open framework to construct accurate real-time wind field using aircraft as sensors.

At first, using our pyModeS library, raw wind vectors are computed from ADS-B and Mode-S down-link data. Then, a novel and fast particle model constructs wind field on a large scale. This model is self-evaluated in order to understand its variability and resistance to errors. The accuracy of calculated wind fields are also validated against GFS data, using data from 28 sets over a long period (one week).

As the result, the combination of accurate wind data from pyModeS and the fast fault resistance particle model is convincing evidence of the utility of open source solutions in ATM research. Our model clearly shows the possibility of using aircraft as large sensor networks to construct a global scale real-time meteorological measuring system under the open-source domain. In stark contrast to the current propitiatory AMDAR system, this model and the results proposed in this paper are fully open to the ATM and the wider scientific community. Without the need for any new equipment or communication protocols, the implementation of such a system is completely based on existing technology and data sources.

References

[1] S. Saha, S. Moorthi, H.-L. Pan, X. Wu, J. Wang, S. Nadiga, P. Tripp, R. Kistler, J. Woollen, D. Behringer *et al.*, "The ncep climate forecast system reanalysis," *Bulletin of the American Meteorological Society*, vol. 91, no. 8, pp. 1015–1057, 2010.

[2] M. Kanamitsu, "Description of the nmc global data assimilation and forecast system," *Weather and Forecasting*, vol. 4, no. 3, pp. 335–342, 1989.

[3] W. R. Moninger, R. D. Mamrosh, and P. M. Pauley, "Automated meteorological reports from commercial aircraft," *Bulletin of the American Meteorological Society*, vol. 84, no. 2, pp. 203–216, 2003.

[4] W. Hollister, E. Bradford, and J. Welch, "Using aircraft radar tracks to estimate wind aloft," *The Lincoln Laboratory Journal*, vol. 2, no. 3, pp. 555–565, 1989.

[5] D. Delahaye, S. Puechmorel, and P. Vacher, "Windfield estimation by radar track kalman filtering and vector spline extrapolation," in *Digital Avionics Systems Conference, 2003. DASC'03. The 22nd*, vol. 1. IEEE, 2003, pp. 5–E.

[6] D. Delahaye and S. Puechmorel, "Aircraft local wind estimation from radar tracker data," in *Control, automation, robotics and vision, 2008. ICARCV 2008. 10th International Conference on*. IEEE, 2008, pp. 1033–1038.

[7] ——, "Tas and wind estimation from radar data," in *Digital Avionics Systems Conference, 2009. DASC'09. IEEE/AIAA 28th*. IEEE, 2009, pp. 2–B.

[8] A. de Leege, M. Van Paassen, and M. Mulder, "Using automatic dependent surveillance-broadcast for meteorological monitoring," *Journal of Aircraft*, 2013.

[9] P. De Jong, J. Van der Laan, M. van Paassen, M. Mulder *et al.*, "Wind-profile estimation using airborne sensors," *Journal of Aircraft*, 2014.

[10] S. de Haan, "High-resolution wind and temperature observations from aircraft tracked by mode-s air traffic control radar," *Journal of Geophysical Research: Atmospheres*, vol. 116, no. D10, 2011.

[11] ——, "Availability and quality of Mode-S MRAR (BDS4. 4) in the MUAC area: a first study," 2014.

[12] M. Hrastovec and F. Solina, "Obtaining meteorological data from aircraft with mode-s radars," *IEEE Aerospace and Electronic Systems Magazine*, vol. 28, no. 12, pp. 12–24, 2013.

[13] S. de Haan, M. de Haij, and J. Sondij, "The use of a commercial ADS-B receiver to derive upper air wind and temperature observations from Mode-S EHS information in The Netherlands," 2013.

[14] C. Hurter, R. Alligier, D. Gianazza, S. Puechmorel, G. Andrienko, and N. Andrienko, "Wind parameters extraction from aircraft trajectories," *Computers, Environment and Urban Systems*, vol. 47, pp. 28–43, 2014.

[15] A. Kapoor, Z. Horvitz, S. Laube, and E. Horvitz, "Airplanes aloft as a sensor network for wind forecasting," in *Proceedings of the 13th international symposium on Information processing in sensor networks*. IEEE Press, 2014, pp. 25–34.

[16] J. Sun, H. Vû, J. Ellerbroek, J. Hoekstra, K. von Hornbostel, T. Robitaille, R. Nobrega, and J. Watterson, "junzis/pymodes v1.2.1," Sep. 2017. [Online]. Available: https://doi.org/10.5281/zenodo.894419